Zi-ang Jin
School of Engineering and Technology,
China University of Geosciences (Beijing),
Beijing 100083, China
e-mail: 15754505018@163.com

Jian-long Ma
National Key Lab for Remanufacturing,
Academy of Armored Forces Engineering,
Beijing 100072, China;
School of Materials Science and Engineering,
Hebei University of Technology,
Tianjin 300130, China
e-mail: majianlong5257@163.com

Li-na Zhu[1]
School of Engineering and Technology,
China University of Geosciences (Beijing),
Beijing 100083, China;
Zhengzhou Institute,
China University of Geosciences (Beijing),
Zhengzhou 451283, China
e-mail: zhulina@cugb.edu.cn

Hai-dou Wang[1]
National Key Lab for Remanufacturing,
Academy of Armored Forces Engineering,
Beijing 100072, China
e-mail: wanghaidou@aliyun.com

Guo-lu Li
School of Materfials Science and Engineering,
Hebei University of Technology,
Tianjin 300130, China
e-mail: liguolu@hebut.edu.cn

Ming Liu
National Key Lab for Remanufacturing,
Academy of Armored Forces Engineering,
Beijing 100072, China
e-mail: hzaam@163.com

Comparison of Dry Sliding Tribological Behavior of Nanostructured Al_2O_3–13 wt% TiO_2 Coatings Prepared by High-Efficiency Supersonic Plasma Spraying and Atmospheric Plasma Spraying

Plasma-sprayed ceramic coatings have been widely used in friction and wear protection of mechanical parts. In this paper, the nanostructured Al_2O_3–13 wt% TiO_2 coatings were prepared by high-efficiency supersonic plasma spraying (HESP) and atmospheric plasma spraying (APS), respectively. The surface and section morphology of the coatings were observed by scanning electron microscopy (SEM). The phase composition of the coatings was analyzed by X-ray diffraction (XRD). The dry sliding friction properties of the coatings were tested on UMT-3 friction and wear testing machine. The results show that after plasma spraying, a large amount of γ-Al_2O_3 phase appears, while the TiO_2 phase almost disappears in the coatings; compared with APS, the coatings sprayed by HESP have fewer defects and better coating quality; under dry friction condition, the steady-state friction coefficient of the coatings sprayed by HESP and APS all decreases with the increase of load, and the wear volume all increases with the increase of load. When the load is more than 40 N, wear volume of the coatings sprayed by APS is basically twice that of HESP; the wear mechanism of the coatings sprayed by HESP is the laminar cracking, peeling off and the adhesive wear.
[DOI: 10.1115/1.4048886]

Keywords: high-efficiency supersonic plasma spraying, nanostructured Al_2O_3–13 wt% TiO_2 coatings, micromorphology, wear mechanism

1 Introduction

Wear is the removal of material from the surface of two objects in contact with each other due to ploughing, adhesion, and so on. Serious wear and failure of parts and components will cause huge economic loss to the productivity of people and even endanger the life safety of people [1–4].

Due to the unique structure with small-size effect, surface effect and quantum size effect, nano materials have better mechanical properties and physical properties than macro materials [5–7]. Nanostructured Al_2O_3–13 wt% TiO_2 coatings is widely used as a wear-resistant coating on the surface of parts because it retains the nanostructure and has the advantages of high strength, high hardness, and good wear resistance [8–11].

As a material surface strengthening technology, plasma spraying makes it possible to spray ceramic materials due to its high heat source temperature (10,000–15,000 °C) [12–14]. However, for atmospheric plasma spraying (APS), although it has a high heat source temperature, it is difficult for the coatings prepared by it to meet the high-performance requirements of parts due to the low particle flying speed [15–17]. For high-efficiency supersonic plasma spraying (HESP), the spray gun adopts a Laval type single anode nozzle, so that the plasma arc is subject to mechanical, self-magnetic, and thermal compression effects in the nozzle to obtain a high-energy density supersonic plasma jet, which can further improve the coatings quality and meet the high-performance requirements of parts [18,19]. At present, relevant researchers have studied the microstructure and mechanical properties of the nanostructured Al_2O_3–13 wt% TiO_2 coatings sprayed by HESP. For example, Li et al. [20] found that the nanostructured Al_2O_3–13 wt% TiO_2 coatings sprayed by HESP have a large number of the metastable γ-Al_2O_3 phase and a small amount of the Al_2TiO_5 phase. The microstructure of the coating has a bimodal distribution including fully melted regions and partially melted regions composed of partially molten particles, solid-phase-sintered regions, liquid-phase-sintered regions, and nanoparticles dispersion-enhanced matrix regions. Li et al. [21] and Wang et al. [22] have both found that the porosity, microhardness, Young's modulus, and fracture toughness of the nanostructured Al_2O_3–13 wt% TiO_2 coatings sprayed by HESP conform to the Weibull distribution and have a large scattering. The microstructure of the coating is composed of completely

[1]Corresponding authors.

Contributed by the Tribology Division of ASME for publication in the JOURNAL OF TRIBOLOGY. Manuscript received May 25, 2020; final manuscript received October 18, 2020; published online November 10, 2020. Assoc. Editor: Thierry Blanchet.

melted regions and partially melted regions. However, no research has been reported on the wear resistance of the nanostructured Al_2O_3–13 wt% TiO_2 coatings sprayed by HESP.

In this paper, the dry sliding tribological properties of nanostructured Al_2O_3–13 wt% TiO_2 coatings sprayed by HESP and APS were evaluated by measuring the friction coefficient and wear volume loss of the coatings under different loading conditions. Moreover, the surface wear morphology of the coating sprayed by HESP was observed and the wear mechanism analyzed.

2 Experimental Materials and Methods

2.1 Preparation of Coatings. The substrate was AISI 1045 steel with the dimensions of 50 mm × 15 mm × 8 mm. The spraying material was the agglomerated nanostructured Al_2O_3–13 wt% TiO_2 composite powder with good spherical shape produced by Tianjin Detianzhu Amorphous Nano Technology Co., Ltd., China (as shown in Fig. 1(*a*)), e the particle size of the powder was mainly distributed in the range of 30–100 μm obtained by the JL-6000 type dry and wet laser particle size analyzer (JL-6000, Chengdu Jingxin, China). The bonding coating was sprayed by Ni–20 wt% Al powder produced by Longquan branch of Chengdu Daguang Thermal Spraying Material Co., Ltd., China, to increase the bonding strength between ceramic coating and metal substrate (as shown in Fig. 1(*b*)).

Before spraying, the substrate needs to be pretreated. The four sides of the substrate were machined chamfer with a length of 1 mm and an angle of 45 deg to reduce the effect of residual stress on the coating performance. The surface was cleaned with alcohol to remove oil stains, and was sandblasted to increase the bonding strength between the coatings and substrate. Finally, the nanostructured Al_2O_3–13 wt% TiO_2 coatings was sprayed by HESP and APS. The HESP was developed by the National Key Laboratory for Remanufacturing, China. As a comparative test, APS was a 50 kW plasma spraying system of the GP-50B type produced by the Jiangxi Jiujiang Best spraying plant. The process parameters of spraying are given in Table 1.

2.2 Characterization of Coatings. The micromorphology of the coating was analyzed by the Nova NanoSEM50-type environmental scanning electron microscope (SEM, FEI, USA), which was equipped with energy-dispersive spectroscopy (OXFORD, UK). The phase structure of the coating was analyzed by an X-ray diffraction (XRD, Bruker, Germany) device with Cu K-alpha radiation. The test parameters were tube voltage 40 kV, current 100 mA, scanning speed 2 deg/min, scanning range 20–80 deg.

2.3 Friction and Wear Test. The dry sliding friction behavior of the coating was tested on a UMT-3 friction and wear tester (CETR, USA), as shown in Fig. 2. Before the test, the surface of the sample was polished to avoid the influence of surface roughness on the tribological properties. Then dry sliding friction is carried out at room temperature and atmospheric relative humidity of 40—50%. The friction pair uses the Si_3N_4 ceramic grinding ball with a diameter of 4 mm and roundness of 0.00016. The specific test parameters are shown in Table 2. Each test parameter was tested three times to ensure the reliability of the data. The LEXT (Olympus OLS4000, Japan) laser three-dimensional microscope was used to observe the three-dimensional morphology of the coating wear scar and to measure the wear volume loss.

3 Results and Discussion

3.1 Micromorphology of Coatings. The surface and cross section micromorphology of the nanostructured Al_2O_3–13 wt% TiO_2 coatings sprayed by HESP and APS are shown in Fig. 3.

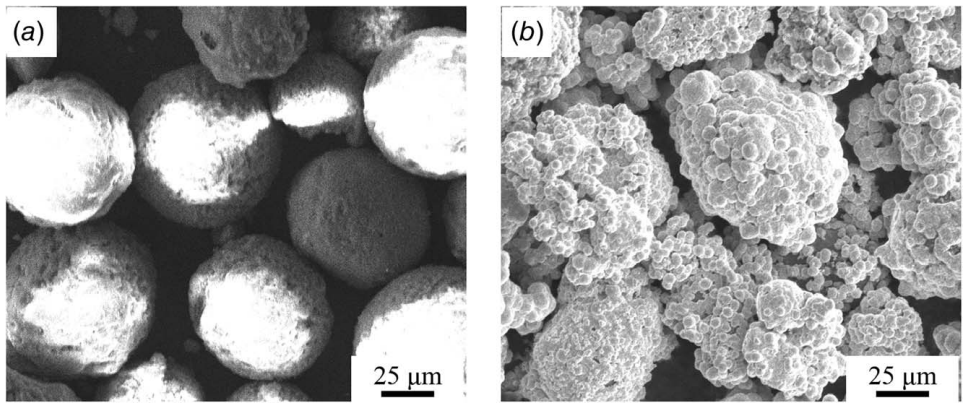

Fig. 1 Microstructure of powder: (*a*) nanostructured Al_2O_3–13 wt% TiO_2 powder and (*b*) Ni–20 wt % Al powder.

Table 1 The process parameters of spraying

Parameters	Ni-20 wt% Al coatings	Nanostructured Al_2O_3–13 wt% TiO_2 coatings-HESP	Nanostructured Al_2O_3–13 wt% TiO_2 coatings-APS
Ar gas flowrate (m^3/h)	3.4	3.2	2.7
H_2 gas flowrate (m^3/h)	—	0.4	—
N_2 gas flowrate (m^3/h)	0.9	—	8.4
Current (A)	360	410	400
Voltage (V)	150	110	95
Powder feed rate (g/min)	40	30	30
Spray distance (mm)	130	100	110
Coating thickness (μm)	50–100	300	300

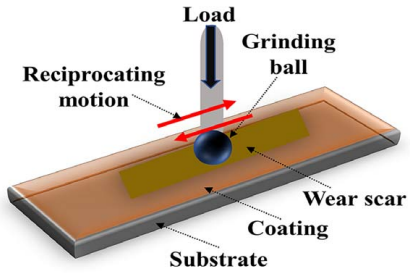

Fig. 2 Reciprocating sliding friction diagram

Table 2 Friction-wear test parameters of nanostructured Al_2O_3–13 wt% TiO_2 coatings

Number	Load (N)	Frequency (Hz)	Amplitude (mm)	Time (min)
1	20	10	4	15
2	30			
3	40			
4	50			
5	60			

As can be seen from Figs. 3(*a*) and 3(*b*), the surface morphology of the coating sprayed by HESP is flat with few pores, while the surface morphology of the APS-sprayed coatings contains a large number of pores and unmelted particles. It also can be seen from Figs. 3(*c*) and 3(*d*) that the cross section morphology of the APS-sprayed coatings contains a large number of different sizes pores, obvious interlayer cracks, and unmelted particles. However, the cross section morphology of the HESP-sprayed coatings only has a few pores, no interlayer cracks, and the coating quality is good. This is due to the high enthalpy and supersonic speed of the HESP jet, which makes the ceramic particles have a better melting state and supersonic flying speed. When they hit the substrate, the deformation of the particles is sufficient, the spreading is uniform, and the coatings quality is better. Therefore, HESP has more advantages in preparing high-quality nanostructured Al_2O_3–13 wt% TiO_2 coatings.

3.2 Phase Composition of Coatings. Figure 4 shows the X-ray diffraction pattern of nanostructured Al_2O_3–13 wt% TiO_2 powder and coatings sprayed by HESP. It can be seen from the figure that the powder is mainly composed of the α-Al_2O_3 phase and rutile-TiO_2 phase. However, after HESP spraying, a large number of γ-Al_2O_3 phases appeared in the coating, while the rutile-TiO_2 phase almost disappeared, which is consistent with the results of the coatings sprayed by APS [14]. This is because the interface energy of γ-Al_2O_3 is lower than that of α-Al_2O_3, so it has lower critical nucleation energy. When the coating is formed by rapid cooling after high temperature plasma spray, the γ-Al_2O_3 phase is preferentially formed [23,24]. At the same time, γ-Al_2O_3 and rutile-TiO_2 react to form a small amount of Al_2TiO_5, which greatly reduces the rutile-TiO_2 phase [25,26].

3.3 Friction and Wear Properties

3.3.1 Friction Coefficient. Figure 5 shows the change curve of the friction coefficient of the coatings sprayed by HESP and APS with time under different load conditions. It can be seen from the

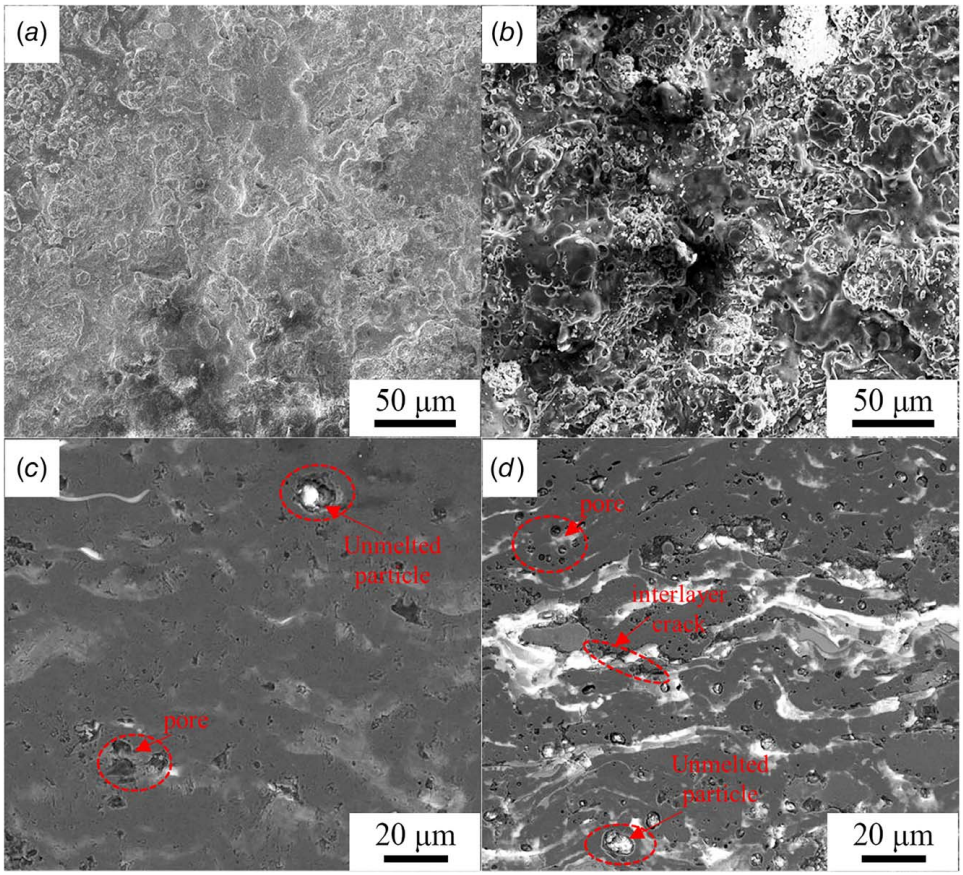

Fig. 3 Micromorphology of nanostructured Al_2O_3–13 wt% TiO_2 coatings: (*a*) surface morphology (HESP), (*b*) surface morphology (APS), (*c*) cross section morphology (HESP), and (*d*) cross section morphology (APS)

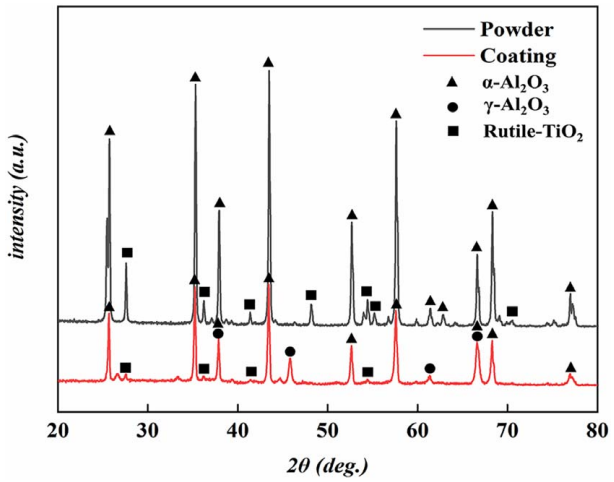

Fig. 4 X-ray diffraction pattern of nanostructured Al_2O_3–13 wt% TiO_2 powder and coatings

figure that the steady-state friction coefficients of the coatings prepared by the two processes all decrease with the increase of the load, and they are between 0.75 and 0.93, which have little difference. In the friction process, the running-in time of the coatings sprayed by APS is much longer than that of HESP from the beginning of friction to the stable friction stage, which takes about 400 s. This is mainly due to the complex and uneven structure of the coatings sprayed by APS, which contains many micro-defects, such as a large number of large size pores and a large proportion of semi-melted regions, resulting in a longer running-in period during the friction process.

3.3.2 Wear Volume. The three-dimensional topographic images of the wear scars of the coatings sprayed by HESP and APS under different applied loads are shown in Fig. 6. With the increase of the applied load, the wear scars become wider and deeper. Also, under the same load conditions, the wear scars of the coatings sprayed by APS are wider and deeper than that of HESP.

Figure 7 shows the relationship between the wear volume loss and the applied load. It can be seen from the figure that the wear volume loss of the coatings sprayed by HESP is always lower than that of APS. When the applied load is lower (<30 N), the wear volume loss of the two coatings is relatively low and there is not much difference. When the applied load is greater than 40 N, the wear volume loss of the coatings sprayed by APS increases sharply, which is basically twice that of the coatings sprayed by HESP, and the test results fluctuate greatly. However, the wear volume loss of the coatings sprayed by HESP increases slowly, and the fluctuation of each test result is small. This is because the coatings sprayed by APS have many micro-defects, and the interlayer bonding and interface bonding are poor. When the applied load is greater than the interlayer bonding force and interface bonding force, the ceramic coatings will crack, peel or collapse, resulting in a large amount of hard abrasive, which will accelerate the friction and wear of the coatings.

3.3.3 Wear Morphology. Figure 8 shows the wear scars morphology of the coatings sprayed by HESP under an applied load of 20 N. It can be seen from Fig. 8(*a*) that the wear scar is shallow (length: 3 mm, width: 0.7 mm). In Fig. 8(*b*), there are a large number of various shapes and sizes of peeling pits and white glass particles shaped like welded nodules on the surface of the wear scar. The coatings have a typical layered structure of thermal spray coating. Under the continuous application of load, cracks generated by stress concentration (as shown in Fig. 8(*c*)), microcracks generated by combining with weak interlayer interface and cracks exist in the coating itself (as shown in Fig. 8(*d*)), which caused the coating of the layered structure to break and separate during the friction period, forming individual spalling pits. The edge of the spalling pits is steep and step-like. Figure 8(*c*) shows the wear scar on the bottom of the spalling pit, where the nanostructures in the partially melted region prevent or deflect crack growth. Figure 8(*d*) shows the ladder fault morphology generated by layer-by-layer cracking of a typical layered structure in the fully molten zone.

Figure 9 shows the wear scars morphology of the coatings sprayed by HESP under applied load of 30 N. It can be seen from Figs. 9(*a*) and 9(*b*) that as the number of spalling pits and welding nodules increases, the volume of each welding nodule becomes larger. As can be seen from Fig. 9(*c*), the layered structure of the coating cracks layer by layer. First, the first layer coating is cracked forming the first layer spalling as shown by the arrow. Then, under repeated application of load, the microcracks and interlayer interface cracks were penetrated and merged by stress concentration resulting in the formation of a second layer spalling. Because the cracks at the bottom of the spalling pit will affect the formation of the lower spalling pit, the coatings will eventually fail due to this repeated action. In Fig. 9(*d*), the typical ladder fault morphology and interlamellar interface cracks are clearly shown.

Figure 10 shows the wear scar morphology of the coatings sprayed by HESP under applied load of 40 N. It can be seen from Fig. 10(*a*) that the width of the wear scar is significantly wider than the wear scar when the load is 20 or 30 N. The area where the welding nodules are piled up becomes larger, and some areas even form large-scale accumulation layers like fish scales, on which there are network-like microcracks (as shown in

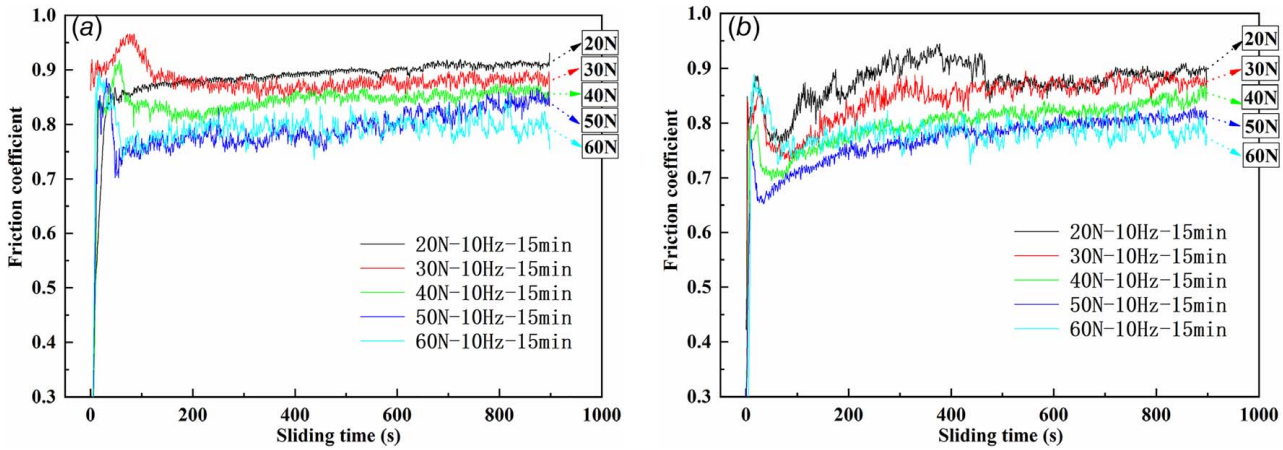

Fig. 5 Friction coefficient of nanostructured Al_2O_3–13 wt% TiO_2 coatings: (*a*) HESP and (*b*) APS

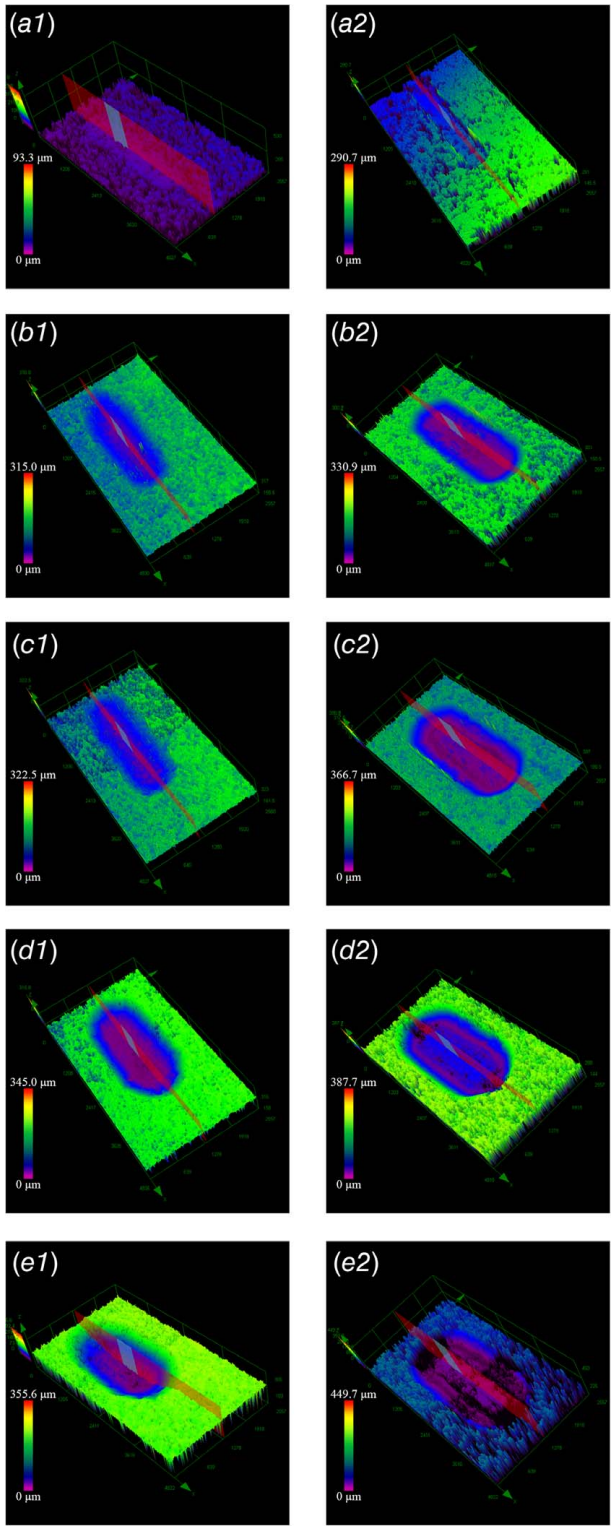

Fig. 6 The three-dimensional topographic images of the wear scars under different applied loads: (*a*) 20 N (a1-HESP, a2-APS); (*b*) 30 N (b1-HESP, b2-APS); (*c*) 40 N (c1-HESP, c2-APS); (*d*) 50 N (d1-HESP, d2-APS); and (*e*) 60 N (e1-HESP, e2-APS)

Figs. 10(*b*) and 10(*c*)). In Fig. 10(*d*), the joint area between the accumulation layer and the grinding surface of the micro-convex body is shown. With the increase in the applied load, the wear of the coating becomes more severe. Due to the surface roughness of the coatings being relatively large, the silicon nitride ceramic

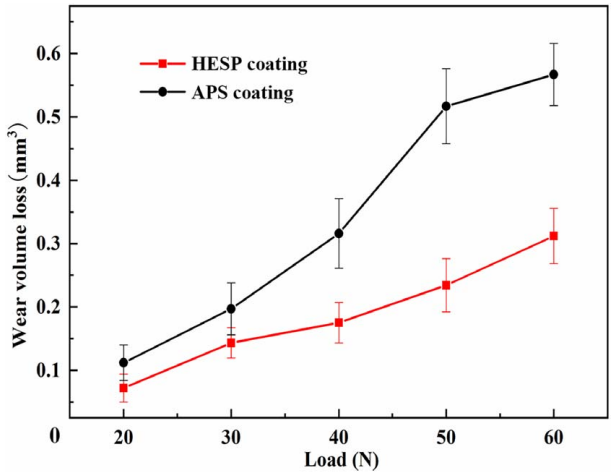

Fig. 7 The relationship between the wear volume loss and the applied load

ball contacts the micro-convex body on the surface of the coatings, generating a large shear stress at its edges, which causes the micro-convex body to break and separate, and then form abrasive debris. At the same time, with the increase of the load, the welding nodules tear and fall off, resulting in wear debris. With the extension of time, these debris may accumulate near the edge of the micro-convex body. Under repeated sliding action, the debris will form a new, dense friction pair containing a large number of nanoparticles to resist the friction and wear together.

Figure 11 shows the wear scars morphology of the coatings sprayed by HESP under an applied load of 60 N. It can be seen from Fig. 11(*a*) that the width of the wear scar is greater than 1 mm. The large area of abrasive debris and welding nodule accumulation layers is almost connected to form a whole piece, forming a new friction pair (as shown in the Figs. 11(*b*)–11(*d*)). The surface of the friction pair is flat and many microcracks are distributed, which are stacked and welded together by a large number of nano and sub-micron particles. With the increase of the load, the formation of a large-area accumulation layer provides new friction pairs for friction and wear, and improves the wear resistance of the coating under heavy load conditions.

3.3.4 Composition of Wear Scar. In the process of friction and wear, sometimes the transfer of materials or the formation of new substances occurs, which has a greater impact on the friction and wear performance [27,28]. Figure 12 shows the element distribution in Fig. 9(*b*) when the applied load is 30 N. As can be seen from Fig. 12, in addition to the three main elements Al, O, and Ti on the surface of the wear scar, there are also Si elements. It was further found that the three elements Al, O, and Ti were distributed uniformly, and the Si element was mainly distributed in the white welding nodule area. This is because under the effect of applied load, the surface elastoplastic deformation is accompanied by the occurrence of high temperature. Under the high temperature and action of pressure welding, element transfer and diffusion occur between the friction pairs, and the Si element on the surface of the grinding ball Si_3N_4 diffuses into the welding nodule areas of the contact area, so a large amount of Si appears in the white welding nodule area.

3.3.5 Wear Mechanism. In the process of friction and wear, the wear resistance of the coating mainly depends on its cohesive bonding strength, toughness, and hardness. The nanostructured Al_2O_3–13 wt% TiO_2 coatings spayed by HESP have higher cohesive strength, toughness, and hardness [21,22], so it has better wear resistance. The wear mechanism of the coatings was lamellar cracking caused by stress-induced cracks, and adhesive wear caused by

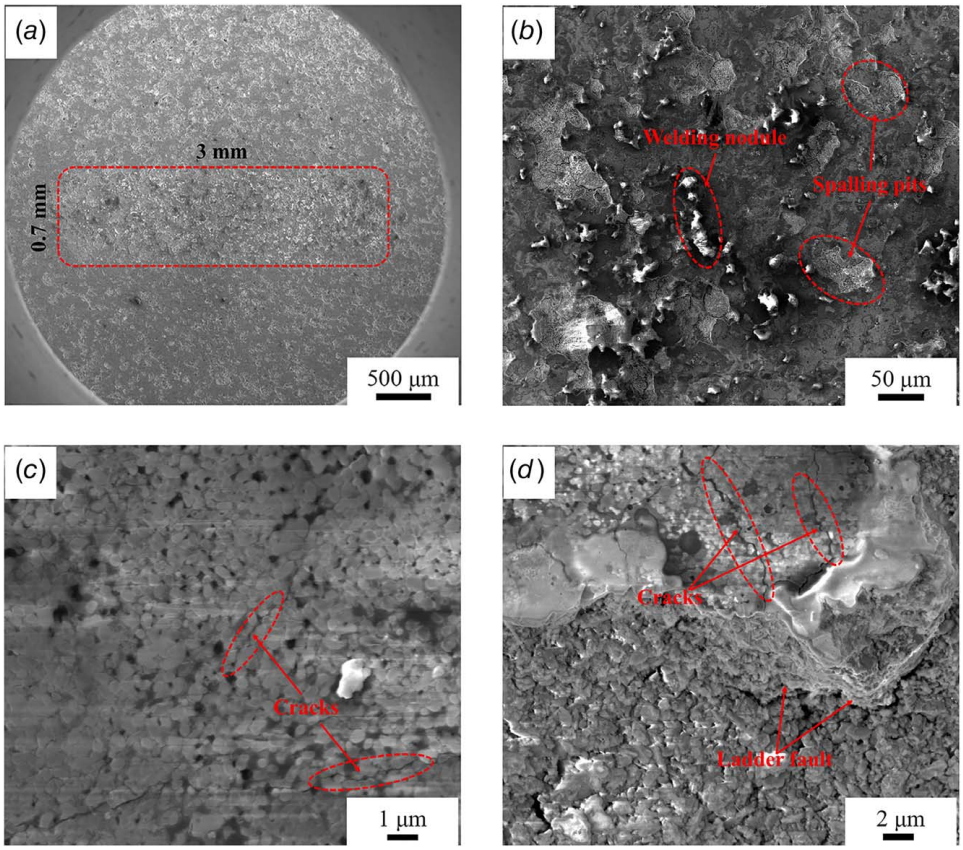

Fig. 8 The wear scars morphology of the coatings sprayed by HESP under a load of 20 N: (*a* and *b*) low magnification and (*c* and *d*) high magnification

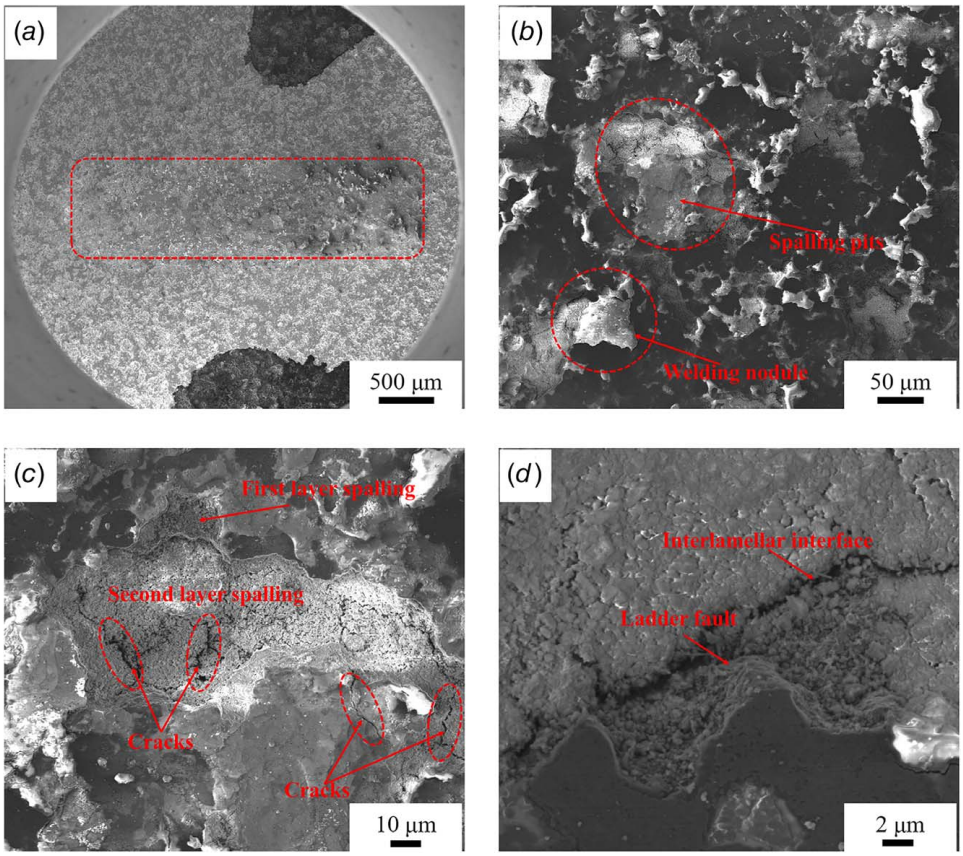

Fig. 9 The wear scars morphology of the coatings sprayed by HESP under a load of 30 N: (*a* and *b*) low magnification and (*c* and *d*) high magnification

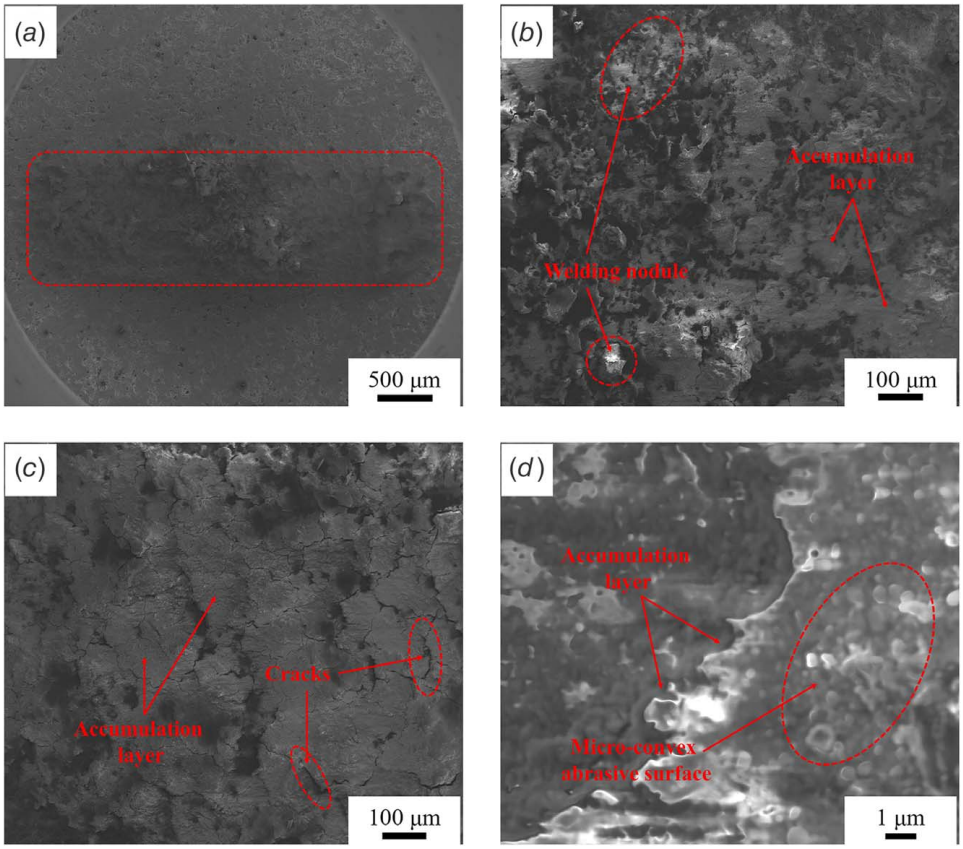

Fig. 10 The wear scars morphology of the coatings sprayed by HESP under a load of 40 N: (*a* and *b*) low magnification and (*c* and *d*) high magnification

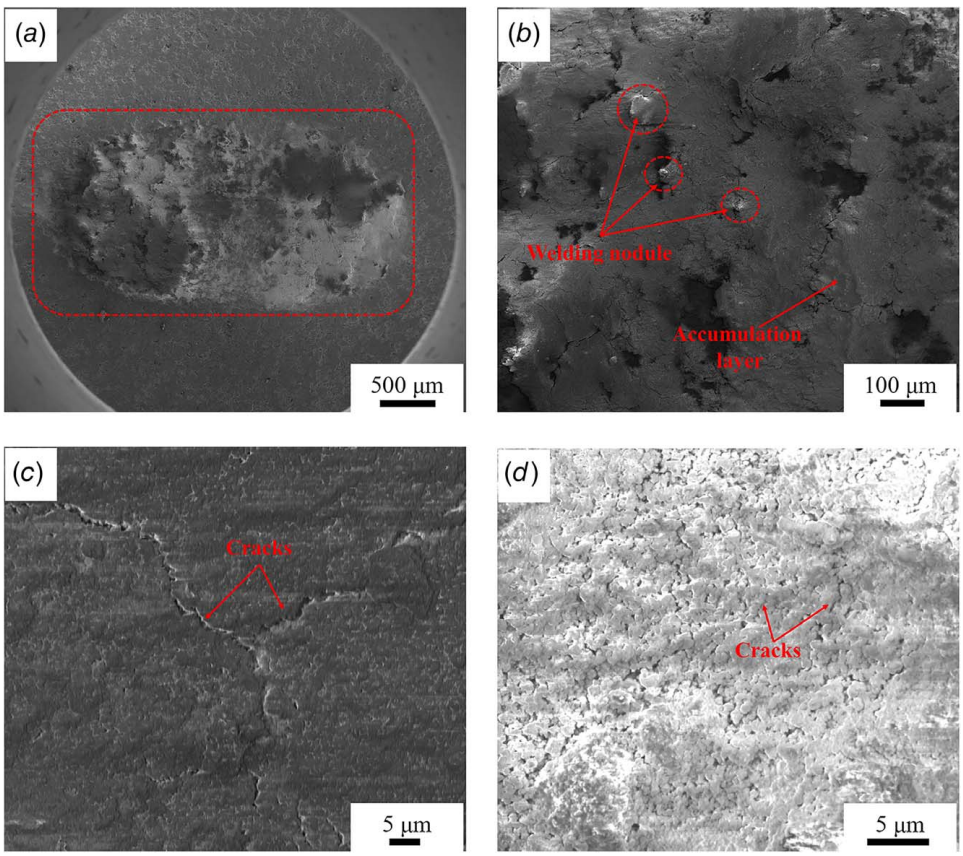

Fig. 11 The wear scars morphology of the coatings sprayed by HESP under a load of 60 N: (*a* and *b*) low magnification and (*c* and *d*) high magnification

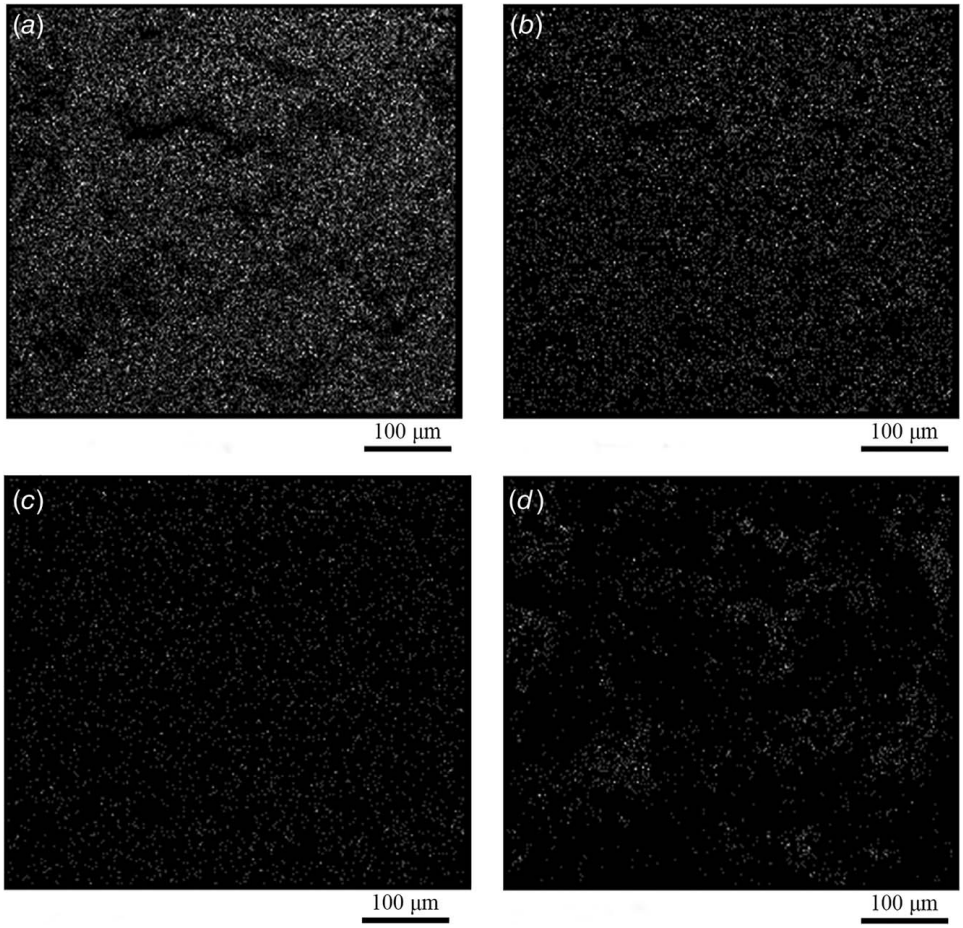

Fig. 12 Element distribution of the wear scars of the coatings sprayed by HESP under a load of 30 N: (*a*) Al, (*b*) O, (*c*) Ti, and (*d*) Si

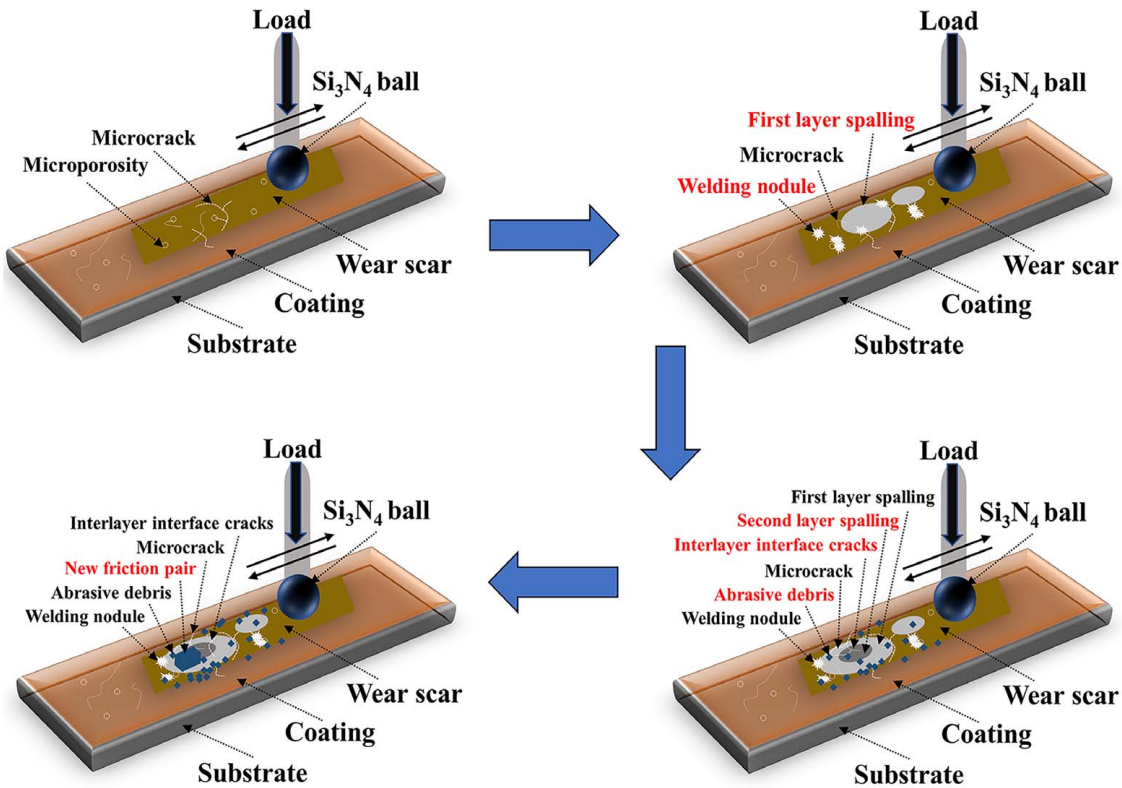

Fig. 13 The wear mechanism of the nanostructured Al_2O_3–13 wt% TiO_2 coatings

frictional high temperature and pressure welding (as shown in Fig. 13). In the process of friction and wear of the coating, under cyclic loading, stress concentration will be generated near the micro-defects (micro-pores or microcracks) of the coatings, promoting the initiation and propagation of microcracks, in which the direction of propagation is random [29,30]. Once these cracks penetrate each other or merge with interlayer interface cracks, the layered structure coatings will be broken and separated layer by layer, forming a stepped edge spalling pit. Under repeated squeezing of the ceramic ball, a large shear stress is generated at the edges of the micro-convex body in the contact area, which causes the micro-convex body to separate from the coating and form abrasive debris. With the increase of the load, due to the effects of frictional high temperature and pressure welding in the contact area, welding nodules are generated, and then the nodules tear and fall off, forming abrasive debris. Under the repeated squeezing action of the ceramic ball, some of these abrasive debris are excluded from the wear scar, and some are accumulated near the edge of the micro-convex body or "pinned" on the friction surface. With the increase of the load, the abrasive debris increases, and a large amount of abrasive debris accumulates in the contact area to form a new friction pair, which reduces the amount of wear and improves its wear resistance under large loads.

4 Conclusions

The following main conclusions were obtained:

(1) Compared with APS, the coatings sprayed by HESP have fewer defects such as pores, cracks, and unmelted particles, in which the coating quality is better. After HESP spraying, a large number of γ-Al_2O_3 phases appear in the coating, while a part of γ-Al_2O_3 reacts with TiO_2 to form a small amount of Al_2TiO_5, and the TiO_2 phase almost disappeared.
(2) Under dry friction condition, the steady-state friction coefficients of the coatings sprayed by HESP and APS all decrease with the increase in load, and they are between 0.75 and 0.93. However, in the process of friction, the time of the coatings sprayed by APS from the initial stage to the friction stable stage is longer than that of HESP.
(3) Under the dry friction condition, the wear volume of the coatings sprayed by HESP and APS all increases with the increase of load; when the load is more than 40 N, the wear volume of the coatings sprayed by APS increases sharply, and under the same load condition, it is basically two times that of HESP, so the wear resistance of the coatings sprayed by HESP is better than that of APS.
(4) Under dry friction, the wear mechanism of the coatings sprayed by HESP is laminar cracking caused by stress concentration-induced cracks and adhesive wear caused by friction high temperature and pressure welding.

Acknowledgment

This work was supported by the National Natural Science Foundation of China (Grant Nos. 41872183 and 51535011), the Pre-Research Program in National 13th Five-Year Plan (Grant No. 61409230603), and the Fundamental Research Funds for Central Universities (Grant No. 2652018095).

Conflict of Interest

There are no conflicts of interest.

References

[1] Pantelis, D. I., Psyllaki, P., and Alexopoulos, N., 2000, "Tribological Behaviour of Plasma-Sprayed Al_2O_3 Coatings Under Severe Wear Conditions," Wear, **237**(2), pp. 197–204.
[2] Shi, Y. N., and Han, Z., 2008, "Tribological Behaviors of Nanostructured Surface Layer Processed by Means of Surface Mechanical Attrition Treatment," Key Eng. Mater., **384**, pp. 321–334.
[3] Grabon, W., Pawlus, P., Wos, S., Koszela, W., and Wieczorowski, M., 2018, "Effects of Cylinder Liner Surface Topography on Friction and Wear of Liner-Ring System at Low Temperature," Tribol. Int., **121**, pp. 148–160.
[4] Wang, G. H., Qu, S. G., XionG, Z. H., Lai, F. Q., Li, X. Q., and Yang, M. S., 2016, "Wear Behaviour and Mechanism of 0.1C-3Cr-2W-V Nitrided Steel Rubbing Against Aluminum Bronze Alloy," J. Iron Steel Res. Int., **23**(3), pp. 281–288.
[5] Goberman, D., Sohn, Y. H., Shaw, L., Jordan, E., and Gell, M., 2002, "Microstructure Development of Al_2O_3–13wt.%TiO_2 Plasma Sprayed Coatings Derived From Nanocrystalline Powders," Acta Mater., **50**(5), pp. 1141–1152.
[6] Wang, D. S., Tian, Z. J., Wang, S. L., Shen, L. D., and Huang, Y. H., 2015, "Solid Particle Erosion Behaviour of Plasma-Sprayed Conventional and Nanostructured Al_2O_3-13 wt% TiO_2 Ceramic Coatings," Trans. Indian Ceram. Soc., **74**(2), pp. 90–96.
[7] Bannier, E., Vicent, M., Rayon, E., Benavente, R., Salvador, M. D., and Sanchez, E., "Effect of TiO_2 Addition on the Microstructure and Nanomechanical Properties of Al_2O_3 Suspension Plasma Sprayed Coatings," Appl. Surf. Sci., **316**, pp. 141–146.
[8] Vicent, M., Bannier, E., Benavente, R., Salvador, M. D., Molina, T., Moreno, R., and Sanchez, E., 2013, "Influence of the Feedstock Characteristics on the Microstructure and Properties of Al_2O_3–TiO_2 Plasma-Sprayed Coatings," Surf. Coat. Technol., **220**, pp. 74–79.
[9] Palanivelu, R., and Kumar, A. R., 2014, "Scratch and Wear Behavior of Plasma Sprayed Nano Ceramics Bilayer Al_2O_3-13 wt%TiO_2/Hydroxyapatite Coated on Medical Grade Titanium Substrates in SBF Environment," Appl. Surf. Sci., **315**, pp. 372–379.
[10] Kang, J. J., Ma, J. L., Li, G. L., Wang, H. D., Xu, B. S., and Wang, C. B., 2014, "Bimodal Distribution Characteristic of Microstructure and Mechanical Properties of Nanostructured Composite Ceramic Coatings Prepared by Supersonic Plasma Spraying," Mater. Des., **64**, pp. 755–759.
[11] Wang, Y., Li, C. G., Guo, L. X., and Tian, W., 2010, "Laser Remelting of Plasma Sprayed Nanostructured Al_2O_3–TiO_2 Coatings at Different Laser Power," Surf. Coat. Technol., **204**(21–22), pp. 3559–3566.
[12] Zhang, J. X., He, J. N., Dong, Y. C., Li, X. Z., and Yan, D. R., 2008, "Microstructure Characteristics of Al_2O_3–13 wt.% TiO_2 Coating Plasma Spray Deposited With Nanocrystalline Powders," J. Mater. Process. Technol., **197**(1–3), pp. 31–35.
[13] Tian, W., Wang, Y., Yang, Y., and Li, C. G., 2009, "Toughening and Strengthening Mechanism of Plasma Sprayed Nanostructured Al_2O_3–13 wt.% TiO_2 Coatings," Surf. Coat. Technol., **204**(5), pp. 642–649.
[14] Wang, D. S., Tian, Z. J., Shen, L. D., Liu, Z. D., and Huang, Y. H., 2009, "Microstructural Characteristics and Formation Mechanism of Al_2O_3–13 wt.% TiO_2 Coatings Plasma-Sprayed With Nanostructured Agglomerated Powders," Surf. Coat. Technol., **203**(10), pp. 1298–1303.
[15] Li, C. G., Wang, Y., Guo, L. X., He, J. Q., Pan, Z. Y., and Wang, L. A., 2010, "Laser Remelting of Plasma-Sprayed Conventional and Nanostructured Al_2O_3–13 wt.%TiO_2 Coatings on Titanium Alloy," J. Alloys Compd., **506**(1), pp. 356–363.
[16] Wang, Y., Li, C. G., Tian, W., and Yang, Y., 2009, "Laser Surface Remelting of Plasma Sprayed Nanostructured Al_2O_3–13wt%TiO_2 Coatings on Titanium Alloy," Appl. Surf. Sci., **255**(20), pp. 8603–8610.
[17] Palacio, C. C., Ageorges, H., Vargas, F., and Diaz, A. F., 2013, "Effect of the Mechanical Properties on Drilling Resistance of Al_2O_3–TiO_2 Coatings Manufactured by Atmospheric Plasma Spraying," Surf. Coat. Technol., **220**, pp. 144–148.
[18] Jin, Z. A., Zhu, L. N., Wang, H. D., Liu, M., Kang, J. J., Ma, G. Z., and Chen, S. Y., 2009, "Microstructures and Wear Resistance of Al-25 wt.%Si Coatings Prepared by High-Efficiency Supersonic Plasma Spraying," J. Therm. Spray Technol., **28**(6), pp. 1308–1317.
[19] Jin, Z. A., Liu, M., Zhu, L. N., Wang, H. D., Ma, G. Z., Xing, Z. G., Kang, J. J., and Chen, S. Y., 2020, "Microstructure and Corrosion Behavior of Aluminum Coatings Prepared by High-Efficiency Supersonic Plasma Spraying and Oxygen–Acetylene Flame Spraying," J. Therm. Spray Technol., **29**(3), pp. 489–499.
[20] Li, L., Kang, J. J., Dong, T. S., Li, G. L., Wang, H. D., and Ma, J. L., 2015, "Formation Mechanism of Supersonic Plasma-Sprayed Nanostructured Composite Ceramic Coatings," Vacuum, **117**, pp. 40–46.
[21] Li, G. L., Ma, J. L., Wang, H. D., Kang, J. J., and Xu, B. S., 2014, "Effects of Argon gas Flow Rate on the Microstructure and Micromechanical Properties of Supersonic Plasma Sprayed Nanostructured Al_2O_3-13wt.%TiO_2 Coatings," Appl. Surf. Sci., **311**, pp. 124–130.
[22] Wang, H. D., Ma, J. L., Li, G. L., Kang, J. J., and Xu, B. S., 2014, "The Dependency of Microstructure and Mechanical Properties of Nanostructured Alumina–Titania Coatings on Critical Plasma Spraying Parameter," Appl. Surf. Sci., **314**, pp. 468–475.
[23] Luo, H., Goberman, D., Shaw, L., and Gell, M., 2003, "Indentation Fracture Behavior of Plasma-Sprayed Nanostructured Al_2O_3–13wt.%TiO_2 Coatings," Mater. Sci. Eng., A., **346**(1–2), pp. 237–245.
[24] Yilmaz, R., Kurt, A. O., Demir, A., and Tatli, Z., 2007, "Effects of TiO_2 on the Mechanical Properties of the Al_2O_3–TiO_2 Plasma Sprayed Coating," J. Eur. Ceram. Soc., **27**(2–3), pp. 1319–1323.
[25] Shaw, L. L., Goberman, D., Ren, R. M., Gell, M., Jiang, S., Wang, Y., Xiao, T. D., and Strutt, P. R., 2000, "The Dependency of Microstructure and

Properties of Nanostructured Coatings on Plasma Spray Conditions," Surf. Coat. Technol., **130**(1), pp. 1–8.
[26] Jordan, E. H., Gell, M., Sohn, Y. H., Goberman, D., Shaw, L., Jiang, S., Wang, M., Xiao, T. D., Wang, Y., and Strutt, P., 2001, "Fabrication and Evaluation of Plasma Sprayed Nanostructured Alumina–Titania Coatings with Superior Properties," Mater. Sci. Eng., A., **301**(1), pp. 80–89.
[27] Cui, S. Y., Miao, Q., Liang, W. P., Zhang, Z. G., Xu, Y., and Ren, B. L., 2017, "Tribological Behavior of Plasma-Sprayed Al_2O_3-20 wt.%TiO_2 Coating," J. Mater. Eng. Perform., **26**(5), pp. 1–9.
[28] Zhao, X. Q., An, Y. L., Hou, G. L., Zhou, H. D., and Chen, J. M., 2014, "Friction and Wear Behavior of Plasma-Sprayed Al_2O_3-13 wt.%TiO_2 Coatings Under the Lubrication of Liquid Paraffin," J. Therm. Spray Technol., **23**(4), pp. 666–675.
[29] Wang, G. H., Qu, S. G., Lai, F. Q., Li, X. Q., Fu, Z. Q., and Yue, W., 2015, "Rolling Contact Fatigue and Wear Properties of 0.1C-3Cr-2W-V Nitrided Steel," Int. J. Fatigue, **77**, pp. 105–114.
[30] Lu, L., Ma, Z., Wang, F. C., and Liu, Y. B., 2013, "Friction and Wear Behaviors of Al_2O_3–13 wt%TiO_2 Coatings," Rare Met., **32**(1), pp. 87–92.